Near Surface Geophysics

EAGE EUROPEAN ASSOCIATION OF GEOSCIENTISTS & ENGINEERS

Near Surface Geophysics, 2018, **16**, 385–399 doi: 10.3997/1873-0604.2017065

Re-parameterisations of the Cole–Cole model for improved spectral inversion of induced polarization data

Gianluca Fiandaca, Line Meldgaard Madsen* and Pradip Kumar Maurya

HydroGeophysics Group, Department of Geoscience, Aarhus University, C.F. Møllers Alle 4, DK-8000 Aarhus C, Denmark

Received January 2017, revision accepted November 2017

ABSTRACT

The induced polarization phenomenon, both in time domain and frequency domain, is often parameterised using the empirical Cole–Cole model. To improve the resolution of model parameters and to decrease the parameter correlations in the inversion process of induced polarization data, we suggest here three re-parameterisations of the Cole–Cole model, namely the maximum phase angle Cole–Cole model, the maximum imaginary conductivity Cole–Cole model, and the minimum imaginary resistivity Cole–Cole model. The maximum phase angle Cole–Cole model uses the maximum phase $\varphi_{\max}$ and the inverse of the phase peak frequency, τ_{φ}, instead of the intrinsic charge-ability m_0 and the time constant adopted in the classic Cole–Cole model. The maximum imaginary conductivity Cole–Cole model uses the maximum imaginary conductivity $\sigma''_{\max}$ instead of m_0 and the time constant τ_{σ} of the Cole–Cole model in its conductivity form. The minimum imaginary resistivity Cole–Cole model uses the minimum imaginary resistivity $\rho''_{\min}$ instead of m_0 and the time constant τ_{ρ} of the Cole–Cole model in its resistivity form.

The effects of the three re-parameterisations have been tested on synthetic time-domain and frequency-domain data using a Markov chain Monte Carlo inversion method, which allows for easy quantification of parameter uncertainty, and on field data using 2D gradient-based inversion. In comparison with the classic Cole–Cole model, it was found that for all the three re-parameterisations, the model parameters are less correlated with each other and, consequently, better resolved for both time-domain and frequency-domain data. The increase in model resolution is particularly significant for models that are poorly resolved using the classic Cole–Cole parameterisation, for instance, for low values of the frequency exponent or with low signal-to-noise ratio. In general, this leads to a significantly deeper depth of investigation for the $\varphi_{\max}$, $\sigma''_{\max}$, and $\rho''_{\min}$ parameters, when compared with the classic m_0 parameter, which is shown with a field example. We believe that the use of re-parameterisations for inverting field data will contribute to narrow the gap between induced polarization theory, laboratory findings, and field applications.

INTRODUCTION

The induced polarization (IP) method is a geophysical technique providing direct sensitivity to the electrical properties of the subsurface at the interface between the rock matrix and the wetting fluid. The method was originally used for mineral exploration, but today, it is frequently applied in environmental surveys where the applications include mapping and characterisation of lithology and soil types (e.g., Slater and Lesmes 2002; Kemna, Binley, and Slater 2004; Johansson *et al.* 2016; Maurya *et al.* 2016) and characterisation of contaminated sites and landfills (e.g., Vanhala 1997; Leroux, Dahlin, and Svensson 2007; Gazoty *et al.* 2012; Johansson, Fiandaca, and Dahlin 2015). Studies have also been investigating the link between the IP effect and the hydraulic properties of the subsurface (e.g., Börner, Schopper, and Weller 1996; Binley *et al.* 2005; Weller *et al.* 2015; Nordsiek *et al.* 2016).

*E-mail: linemeldgaard@geo.au.dk

In time domain (TD), the IP phenomenon manifests itself as a transient potential rise/decay following the switch on/off of an electric current induced through a medium. In frequency domain (FD), this corresponds to a phase shift between the applied current and the arising potential. The IP effect of a material can thus be described by a frequency-dependent complex electrical resistivity. However, no universal physical model is available to describe the effect and IP is often parameterised using phenomenological models.

The classic Debye model describes the simplest form of a dielectric relaxation response to an alternating current. Cole and Cole (1941) extended the Debye model to account for new experimental observations on different materials. The original Cole–Cole model, expressed in terms of a complex dielectric constant, was later rewritten by Pelton *et al.* (1978) to describe the complex resistivity response of mineralised rocks. A complex conductivity form of the original Cole–Cole model is often encountered in literature as well (e.g., Tarasov and Titov 2013).

Today, the Cole–Cole model (in resistivity or conductivity form) is one of the most prevailing models used for parameterisation and inversion of TD IP data (e.g., Yuval and Oldenburg 1997; Hönig and Tezkan 2007; Fiandaca *et al.* 2012), as well as FD IP data (e.g., Yoshioka and Zhdanov 2005; Loke, Chambers, and Ogilvy 2006).

Madsen *et al.* (2017) presented a sensitivity analysis of Cole–Cole parameters retrieved from TD IP data. In this study, the Cole–Cole model (resistivity form) was used in terms of the following parameters: the direct current resistivity (ρ_0), the intrinsic chargeability (m_0) as described by Seigel (1959), the relaxation time (τ_ρ), and the frequency exponent (C). Here, the τ_ρ symbol is used instead of the classic τ symbol for stressing the fact that τ_ρ refers to the resistivity Cole–Cole model.

The sensitivity analysis proved that spectral Cole–Cole parameters can be retrieved from TD IP data when using fulldecay data and an acquisition range above 2.5 decades in time and that the resolution of the Cole–Cole parameters decreases significantly for small values of C and for values of τ_ρ far outside the acquisition range (Madsen *et al.* 2017). Furthermore, a strong correlation between m_0 and C was detected in both synthetic generated data and field data. The correlation between m_0 and C has also been detected from inversion of FD IP data (Bérubé *et al.* 2017).

To improve the model resolution retrieved from inversion of IP data, we suggest three re-parameterisations of the Cole–Cole model: the maximum phase angle (MPA) Cole–Cole model, the maximum imaginary conductivity (MIC) Cole–Cole model, and the Minimum Imaginary Resistivity (MIR) Cole–Cole model. The sensitivity of the classic and the new Cole–Cole model parameters are compared using Markov chain Monte Carlo (MCMC) inversion, which allows us to study the posterior probability distributions of each parameter and quantify uncertainties without linearisation. We show that models, which are poorly resolved from inversion with the classic Cole–Cole model (e.g., due to low signal-to-noise ratio) can be resolved well with the new re-parameterisations and that the re-parameterisations work equally well for TD and FDIP data. In addition, we present a field example that shows that gradient-based inversions benefit from the re-parameterisations as well and consequently obtain a significantly deeper depth of investigation.

RE-PARAMETRISATIONS OF COLE–COLE

The Cole–Cole model describing the complex resistivity is defined as follows (Pelton *et al.* 1978):

$$\tilde{\rho}(\omega) = \rho'(\omega) + i\rho''(\omega) = \rho_0 \left[1 - m_0 \left(1 - \frac{1}{1 + (i\omega\tau_\rho)^C} \right) \right], \quad (1)$$

where ρ_0, m_0, τ_ρ, and C are the previously described Cole–Cole parameters, $\omega = 2\pi f$ is the angular frequency, and i is the imaginary unit. The model space is thus defined as follows:

$$\boldsymbol{m}_{resistivity\ Cole-Cole} = \{\rho_0, m_0, \tau_\rho, C\}. \quad (2)$$

Alternatively, the Cole–Cole model can also be presented in its conductivity form (e.g., Tarasov and Titov 2013), as follows:

$$\tilde{\sigma}(\omega) = \sigma'(\omega) + i\sigma''(\omega) = \sigma_0 \left[1 - \frac{m_0}{1 - m_0} \left(1 - \frac{1}{1 + (i\omega\tau_\sigma)^C} \right) \right], \quad (3)$$

with the corresponding model space defined as follows:

$$\boldsymbol{m}_{\text{conductivity Cole–Cole}} = \{\sigma_0, m_0, \tau_\sigma, C\}. \quad (4)$$

The conductivity and resistivity Cole–Cole models (CCC and RCC, respectively) are identical, i.e., $\tilde{\sigma}(\omega) = 1/\tilde{\rho}(\omega)$, when the respective relaxation times τ_σ and τ_ρ obey the following relation:

$$\tau_\sigma = \tau_\rho \cdot (1 - m_0)^{1/C} \quad (5)$$

The inverse of τ_σ represents the angular frequency of the maximum of the imaginary conductivity, as follows:

$$\sigma''_{\max} = \sigma''(\omega = 1/\tau_\sigma), \quad (6)$$

whereas the inverse of τ_ρ represents the angular frequency of the minimum of the imaginary resistivity, as follows:

$$\rho''_{\min} = \rho''(\omega = 1/\tau_\rho). \quad (7)$$

Figure 1 shows the absolute value of the complex resistivity $|\tilde{\rho}|$, the phase of the complex conductivity φ, the imaginary

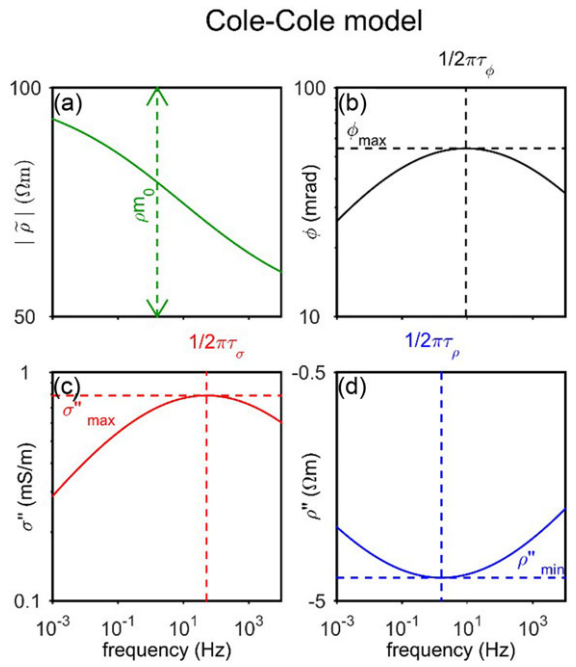

Figure 1 Cole–Cole model defined by $\rho_0 = 100\Omega$m, $m_0 = 500$ mV/V, $\tau_\rho = 0.1\,s$, and $C = 0.2$. (a) Amplitude of the complex resistivity; (b) phase of the complex conductivity; (c) imaginary conductivity; (d) imaginary resistivity.

conductivity σ'', and the imaginary resistivity ρ'' of the Cole–Cole model as a function of frequency for the model defined by $\rho_0 = 100\ \Omega m$, $m_0 = 500\ mV/V$, $\tau_\rho = 0.1\ s$, and $C = 0.2$. The high m_0-value was chosen to emphasise the frequency variation of the spectrum.

The phase of the complex conductivity, $\varphi(\omega)$ (Fig. 1b), can be defined in terms of both equation (1) and equation (3), so

$$\varphi(\omega) = \tan^{-1}\left(\frac{\sigma''(\omega)}{\sigma'(\omega)}\right) = -\tan^{-1}\left(\frac{\rho''(\omega)}{\rho'(\omega)}\right). \tag{8}$$

The phase reaches a maximum, φ_{max}, at an angular frequency $\omega_\varphi = 1/\tau_\varphi$ (Fig. 1b), as follows:

$$\varphi_{max} = \tan^{-1}\left(\frac{\sigma''(1/\tau_\varphi)}{\sigma'(1/\tau_\varphi)}\right) = -\tan^{-1}\left(\frac{\rho''(1/\tau_\varphi)}{\rho'(1/\tau_\varphi)}\right), \tag{9}$$

where the relaxation time, τ_φ, is linked to τ_ρ and τ_σ through the other Cole–Cole parameters m_0 and C, as follows:

$$\tau_\varphi = \tau_\rho \cdot (1 - m_0)^{1/2C} = \tau_\sigma \cdot (1 - m_0)^{-1/2C}. \tag{10}$$

The differences among τ_ρ, τ_σ, and τ_φ increase with an increase of m_0 and/or with a decrease of C. Furthermore. φ_{max}, as well as σ''_{max} and σ''_{min}, increases with m_0 and C. The dependence of the phase shift on both m_0 and C is the main reason for the parameter correlations described by Madsen *et al.* (2017) and Bérubé *et al.* (2017), as depicted in Fig. 2. In fact, with frequency ranges below 4 decades. which is typical in field IP surveying; similar variations in the phase spectrum can be induced by decreasing m_0 (magenta line, Fig. 2a) or C (blue line, Fig. 2a). A similar equivalence is found in TD, with acquisition ranges below 4 decades (Fig. 2b). However. it has to be noted that in order to take the acquisition range in the TD forward response into account. the current waveform. and particularly the duration of the current injection. has to be modelled. This explains the difference between the step response (dashed black line) and the response with limited acquisition range (continuous black line) in Fig. 2b.

Maximum phase angle

We suggest a re-parameterisation of the Cole–Cole model where instead of m_0 and τ_ρ, the maximum phase φ_{max} (equation (9) and Fig. 1b) and the phase relaxation time τ_φ (equation (10) and Fig. 1b) are used as model parameters. The re-parameterised model space becomes as follows:

$$\boldsymbol{m}_{\text{MPA Cole–Cole}} = \{\rho_0, \varphi_{max}, \tau_\varphi, C\}. \tag{11}$$

In Fig. 2c, the variations in the phase spectrum induced by a decrease of φ_{max} (blue line) and an increase of C (green line) are shown. In comparison with the classic Cole–Cole parameterisation (Fig. 2a), a much bigger data difference is present between the responses, meaning that φ_{max} and C are less correlated than m_0 and C. The same applies in the comparison of the TD responses in Fig. 2b and Fig. 2d. In TD, we see that the green response (C 30% decrease) follows the reference model at the early time and the blue response (φ_{max} 30% decrease) at the late times (Fig. 2d).

To summarise, the parameter φ_{max} controls the FD maximum phase shift and the magnitude of the TD decays, whereas the parameter C controls the width of the phase shift and the decay shape.

Given the maximum phase angle (MPA) Cole–Cole model parameters $\{\rho_0, \varphi_{max}, \tau_\varphi, C\}$, the corresponding parameters of the RCC (or CCC) model $\{\rho_0, m_0, \tau_\rho, C\}$ can be easily computed through an iterative approach (See Appendix A).

Maximum imaginary conductivity

Another re-parameterisation of the classic Cole–Cole model is the MIC Cole–Cole model. The MIC model space is defined in terms of the following:

$$\boldsymbol{m}_{\text{MIC Cole–Cole}} = \{\sigma_0, \sigma''_{max}, \tau_\sigma, C\}, \tag{12}$$

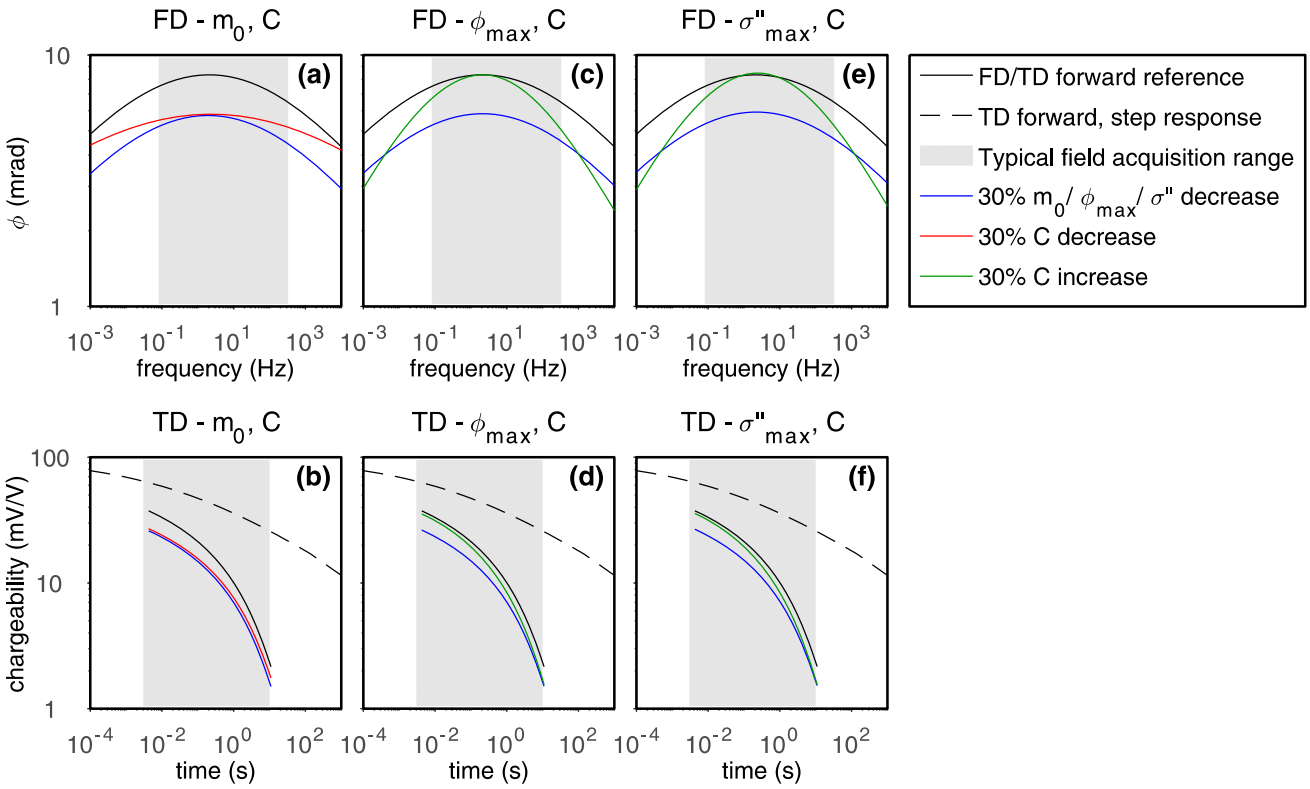

Figure 2 Variations of FD and TD responses with m_0, $\varphi_{\max}$, $\sigma_{\max}$, and C. Reference model: $\rho_0 = 100\ \Omega m$, $m_0 = 100$ mV/V, $\tau_\rho = 0.1\,s$, and $C = 0.2$. (a) FD responses, m_0, and C variations; (b) TD responses, m_0 and C variations; (c) FD responses, $\varphi_{\max}$, and C variations; (d) TD responses, $\varphi_{\max}$, and C variations; (e) FD responses, $\sigma''_{\max}$, and C variations; (f) TD responses, $\sigma''_{\max}$, and C variations.

where $\sigma''_{\max}$ is the maximum of the imaginary conductivity (Fig. 1c) as defined in equation (6).

The influence of changes in $\sigma''_{\max}$ and C on the phase shift and the chargeability is shown in Fig. 2e and Fig. 2f, respectively. The responses are very similar to those of $\varphi_{\max}$, because $\sigma''_{\max} \cong \sigma_0 \varphi_{\max}$. Given the MIC Cole–Cole model parameters, the corresponding parameters of the CCC models can be computed directly as shown in Appendix A.

Minimum imaginary resistivity

The resistivity equivalence to the MIC Cole–Cole model is the minimum imaginary resistivity MIR Cole–Cole model. The model space is defined in terms of the following:

$$\boldsymbol{m}_{\text{MIR Cole–Cole}} = \{\rho_0, \rho''_{min}, \tau_\rho, C\}, \tag{13}$$

where ρ''_{min} is the minimum of the imaginary resistivity (Fig. 1d) as defined in equation (7). The responses of the MIR Cole–Cole model are not shown in Fig. 2 as they are similar to those of $\varphi_{\max}$ and $\sigma''_{\max}$ because $\rho''_{\min} \cong -\rho_0 \phi_{\max}$.

Given the MIR Cole–Cole model parameters, the corresponding parameters of the RCC model can be computed directly as shown in Appendix A.

DATA SPACE

Time-domain data

The data space, $\boldsymbol{d}_{\text{obs}}$, for the MCMC and gradient-based inversions of TD IP data consists of apparent resistivity and full-decay chargeability values, as follows:

$$\boldsymbol{d}_{\text{obs}} = \{\rho_a, M_i\}, i = 1 : N_{gates} \tag{14}$$

Where ρ_a (Ωm) is the apparent resistivity, and the data-space chargeability, M_i (mV/V), is computed in each time gate, i, of the transient full-decay IP signal as described by Olsson *et al.* (2015). If no negative data are present, the inversion can be performed in logarithmic data space.

A waveform with a 100% duty cycle, where the TD IP data are measured in the current-on time as described by Olsson *et al.* (2015), is applied for both the generation of

synthetic data and in the field data acquisition. For the synthetic data, each IP signal is recorded from 2.6 ms to 12,000 ms, and the decay is divided into 26 time gates (listed in Appendix B) with an approximately logincreasing gate width to improve the signal-to-noise ratio at late times (Fiandaca *et al.* 2012). The same acquisition range (about 3.5 decades) is also obtainable in field surveying when full-waveform recordings are processed for harmonic de-noising and background removal (see details in the field example). Three stacks have been modelled in the synthetic forward responses, whereas two stacks have been used in the field example. The used quadrupoles and the noise model are described in separate results section for the synthetic data and field data.

Frequency-domain data

For the FD IP data, the data space consists of the amplitude, A_j (Ωm), and the data-space phase, φ_j (mrad), which are measured at a range of frequencies, j. Similar to the phase defined in model space, the data-space phase is defined here as the phase of the complex conductivity. The data vector applied in the inversion becomes the following:

$$\boldsymbol{d}_{\text{obs}} = \{\varphi_j, A_j\},\ j = 1 : N_{\text{frequencies}}. \tag{15}$$

For the synthetic data, we simulate measurements at 13 frequencies in the range from 0.08 Hz to 327 Hz and thereby get 26 data values in total, the same as the number of time gates applied in TD. In total, about 3.5 decades in frequency are spanned by the data, with the first and last frequencies approximately equal to the inverse of the last and first TD center gate time, respectively. The applied frequencies are listed in Appendix B. Used quadrupoles and noise model are described in the results section.

INVERSION METHODOLOGY

The 1D TD forward response of synthetic data is computed using the algorithm presented by Fiandaca *et al.* (2012). This algorithm computes the full-decay IP response and models the transmitter current waveform and the receiver transfer function accurately. The same algorithm has been applied to compute the FD forward response by disregarding the TD transform. An extension of the algorithm, which computes the 2D forward response (Fiandaca *et al.* 2013), has been applied in the inversion of field data.

In the following analyses of the re-parameterisations of the Cole–Cole model, we have used two different inversion methods. First, an MCMC inversion algorithm is used to compute a non-linearised uncertainty analysis of all the model parameters. Hereafter, a field example is inverted in 2D using a gradient-based inversion approach in order to show how field surveys may benefit from the re-parameterisations.

Markov chain Monte Carlo inversion

With the MCMC inversion method, it is possible to investigate the distribution of models that fit a given dataset. Compared with a gradient-based inversion, the MCMC method (as well as other statistical inversion approaches) has an advantage when it comes to quantifying parameter uncertainties and correlations without linearising the problem as described by Chen, Kemna, and Hubbard (2008) and Madsen *et al.* (2017).

In this study, we apply a Metropolis–Hastings sampling algorithm (Metropolis *et al.* 1953; Hastings 1970) that, based on a random walk in the model space, samples models according to their likelihood. The sampled models make up a Markov chain, which converges towards the posterior probability distribution of the model space.

The applied sampling algorithm, which is described in detail by Madsen *et al.* (2017), works in two steps. First, a model is proposed. Next, the model is accepted to the Markov chain with an acceptance probability that depends only on the last accepted model in the chain and none of the previous models. These two steps are repeated for a predefined number of times or until the distribution of the sampled models (the posterior probability distribution) has converged.

Because we apply a symmetric model proposer, where the possibility of walking from model $\boldsymbol{m}_i$ to $\boldsymbol{m}_j$ is the same as walking from $\boldsymbol{m}_j$ to $\boldsymbol{m}_i$, the acceptance probability of $\boldsymbol{m}_i$ can be computed simply as a likelihood ratio (Malinverno, 2002) as follows:

$$P_{acc}(\boldsymbol{m}_i) = min\left[1, \frac{P_{like}(\boldsymbol{m}_i)}{P_{like}(\boldsymbol{m}_{i-1})}\right], \tag{16}$$

where the likelihood function is given by Mosegaard and Tarantola (2002) as follows:

$$P_{like}(\boldsymbol{m}) = k \cdot \exp\left[\frac{1}{2}(g(\boldsymbol{m}) - \boldsymbol{d}_{\text{obs}})^T \boldsymbol{C}_{\text{obs}}(g(\boldsymbol{m}) - \boldsymbol{d}_{\text{obs}})\right], \tag{17}$$

where g($\boldsymbol{m}$) is the forward response of the model $\boldsymbol{m}$, $\boldsymbol{C}_{obs}$ is the covariance matrix of the observed data, $\boldsymbol{d}_{obs}$, and k is a normalisation constant.

Due to the logarithmic transform applied on the model parameters, uncertainties are given as standard deviation factors (STDFs), where the STDF of the marginal posterior

probability distribution, *PDF* (defined in the logarithmic space), can be computed as follows:

$$STDF = exp(STD(PDF)). \tag{18}$$

Assuming that the model parameters are normally distributed in the logarithmic space, we get the following ±STD limits:

$$\frac{\mu}{STDF} < \mu < \mu \cdot STDF, \tag{19}$$

where μ is the mean of the distribution. So, with $STDF = 1.1$, the model parameter has a relative uncertainty of 10%, whereas with $STDF = 2.0$, the uncertainty grows 10-fold to 100%. Using the terminology of Auken *et al.* (2005), an STDF < 1.2 is a well-resolved parameter, $1.2 <$ STDF < 1.5 is a moderately resolved parameter, $1.5 <$ STDF < 2 is a poorly resolved parameter, and STDF > 2 is an unresolved parameter.

The posterior distribution of the classic Cole–Cole parameters is related to the ones of the re-parameterisations. In theory, with a complete knowledge of the posterior distribution of the Cole–Cole model (including the asymptotic behavior) and an analytical expression for the mapping between the parameterisations, it would be possible to obtain the posterior distribution of the re-parameterisation from the one of the classic Cole–Cole. This is difficult to obtain in practice, which is why we have chosen to sample the distributions for each parameterisation individually.

Gradient-based inversion

For inversion of field data, we apply the gradient-based 2D inversion scheme that is described in detail by Fiandaca *et al.* (2013). The algorithm applies the first term Taylor expansion for linearisation and uses an iterative method to minimise the misfit, as follows:

$$\chi = \left(\frac{\delta \boldsymbol{d}^T \mathbf{C}_{\text{obs}}^{-1} \delta \boldsymbol{d} + \delta \boldsymbol{r}^T \mathbf{C}_R^{-1} \delta \boldsymbol{r}}{N_d + N_R} \right)^{\frac{1}{2}}, \tag{20}$$

where $\delta \boldsymbol{d}$ is the data misfit, $\mathbf{C}_{\text{obs}}$ is the covariance matrix of the observed data, $\delta \boldsymbol{r}$ is the model roughness, and $\mathbf{C}_R$ is the covariance on the roughness constraints. N_d and N_R are the numbers of data parameters and roughness constrains, respectively. No priors have been used in the inversion; however, if priors were applied, this would add an extra term to equation (20).

From the inversion result, a linearised uncertainty analysis is computed based on the posterior covariance matrix (Tarantola and Valette 1982), as follows:

$$\mathbf{C}_{est} = \left(\boldsymbol{G}^T {\mathbf{C}_{\text{obs}}}^{-1} \boldsymbol{G} + \boldsymbol{R}^T {\mathbf{C}_R}^{-1} \boldsymbol{R} \right)^{-1}, \tag{21}$$

where $\boldsymbol{G}$ is the Jacobian matrix holding the partial derivatives of the mapping and $\boldsymbol{R}$ is the roughness matrix. Equivalent to the uncertainty analysis in the MCMC approach (equations (18) and (19)), we computed an STDF of the ith model parameter m_i as follows:

$$\text{STDF}(m_i) = \exp\left(\sqrt{C_{est(i,i)}} \right). \tag{22}$$

The STDFs computed for the gradient-based inversion (using equations (21) and (22)) are influenced by the values of the roughness constrains, which is why they should only be seen as a relative measure of the uncertainty and cannot be directly compared with the STDFs of constraint-free inversions (either MCMC or other gradient-based results).

Alongside the linearised uncertainty analysis in terms of STDFs, the DOI of the inversion model is computed. The DOI algorithm used in this study is based on a cumulated approximated analysis (CAA) that incorporates the actual output model from the inversion and the data errors, as described by Fiandaca, Christiansen, and Auken (2015). For a given depth D, the CAA computes the data-driven (i.e., $\boldsymbol{C}_R = 0$) in equation (21)) cumulated uncertainty analysis, model column by model column. This is done by cumulating the sensitivity of all the model cells below the depth D. A threshold value for the STDF of the CAA is defined, and the DOI is computed as the depth at which this threshold is reached. Based on experience, DOI threshold values between 2 and 5 give reasonable DOI estimations. The values of the DOI threshold are usually increased for the τ parameter, which is significantly less resolved and for which the order of magnitude is of interest even when the parameter resolution is low. In this study, the DOI threshold is STDF = 4 for all parameter except τ, for which STDF = 20. The approximation in the CAA algorithm consists of neglecting the correlations between model parameters belonging to different model columns (lateral data correlation) but still considering the correlation among the Cole–Cole parameters for each model column. This means that the DOI algorithm gives results that depend on the actual model parameterisation used in the inversion and can thus be used as a comparative factor between the parameters of different Cole–Cole parameterisations.

UNCERTAINTY ANALYSIS

In the following, we present the results of an uncertainty analysis computed using MCMC methods. The MCMC inversion results are presented as marginal posterior probability distributions, which are the distributions of the sampled models shown for each individual model parameter, and the

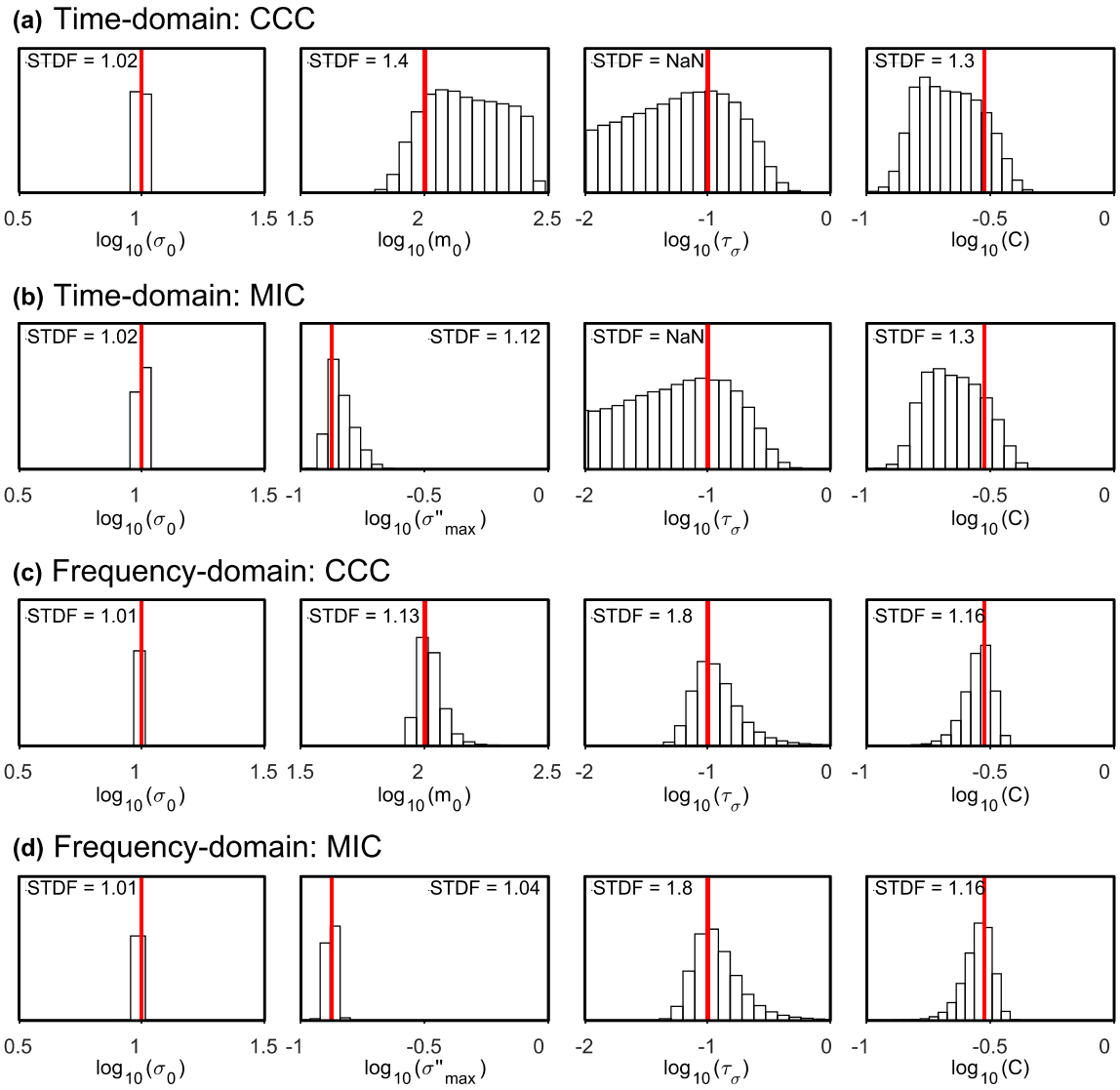

Figure 3 Posterior probability distributions of a homogenous half-space model with the parameters: $\sigma_0 = 10$ mS/m, $m_0 = 100$ mV/V ($\sigma''_{\max} = 0.13$ mS/m), $\tau_\sigma = 0.1$ *s*, and $C = 0.3$. The distributions are shown for (a) TD, conductivity Cole–Cole; (b) TD, MIC Cole–Cole; (c) FD, conductivity Cole–Cole; and (d) FD, MIC Cole–Cole. The red line marks the true model. NaN indicates that the distribution has not converged. Note that the distributions of τ_σ are wider scaled.

uncertainty is given as the STDF of each distribution as defined in equation (18).

The applied noise model has a relative and an absolute term, for both TD and FD data. In TD, a 2% standard deviation has been applied to the resistivity data; 10% relative standard deviation plus 0.2 mV/V absolute noise has been applied on the IP data. Similarly, in FD, a 2% standard deviation is considered for the amplitude data; 10% relative standard deviation plus 0.2 mrad absolute noise has been applied on the phase data.

A homogenous half-space example

Synthetic data have been generated from a homogenous half-space model using one quadrupole with electrode spacing $|AB| = 7.5$ m and $|MN| = 2.5$ m.

Five different parameterisations have been investigated: the classic CCC and RCC, and the three new re-parameterisations (MPA, MIC, MIR). The values of the parameters for all parameterisations were derived from the CCC model: $\sigma_0 = 10$ mS/m, $m_0 = 100$ mV/V, $\tau_\sigma = 0.1$ *s*, and $C = 0.2$. MCMC inversions of TD and FD synthetic data

were performed for each parameterisation individually using five MCMC runs with different starting models and with one million model proposes (iterations) in each run.

For both TD and FD, the inversion results from the CCC model and the MIC Cole–Cole model are presented in Fig. 3. The posterior probability distributions are plotted together with the true model (red line) and the STDFs.

For both TD and FD, the resolutions of σ_0, τ_σ, and C are the same and independent of the parameterisation (Fig. 3). However, the resolution of $\sigma''_{\max}$ is significantly better than the resolution of m_0. As given by the STDFs, it is approximately a 3-fold improvement in both TD (from STDF = 1.4 to STDF = 1.12) and FD (from STDF = 1.13 to STDF = 1.04). The results of the MPA and the MIR model are very similar to those of the MIC, which is why they are not shown here; however, the STDFs are listed in Table 1. Overall, the results show that the FD data give a better resolved than the TD data. This is due to the choice of the relaxation time ($\tau_\sigma = 0.1$). If we instead set $\tau_\sigma = 1$, the TD data give the best resolution (see Discussion).

Figure 4 shows the cross-plots of m_0 and $\sigma''_{\max}$ with the remaining Cole–Cole parameters. A non-linear correlation is present between m_0 and τ_σ (Fig. 4b), whereas the correlation between $\sigma''_{\max}$ and τ_σ is linear and spans a smaller area of the model space (Fig. 4e). The correlation between C and m_0 or $\sigma''_{\max}$ are both non-linear, but we see that $\sigma''_{\max}$ spans a smaller parameter range. Consequently, $\sigma''_{\max}$ is resolved better than m_0.

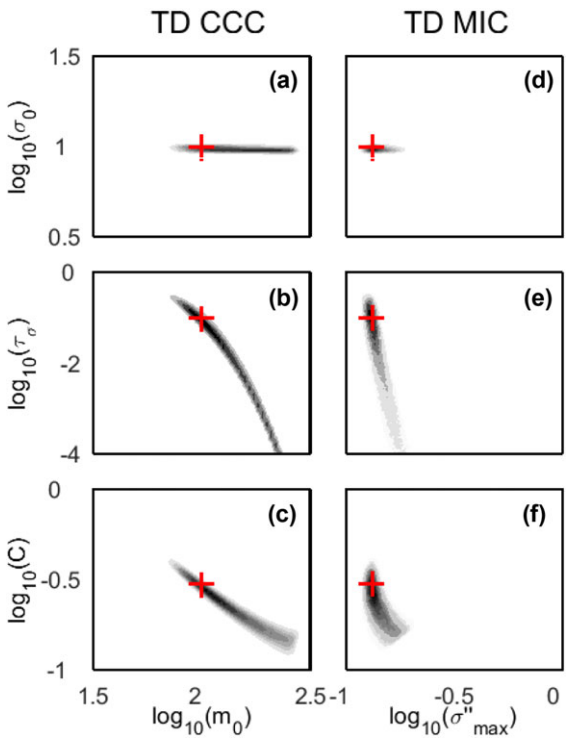

Figure 4 Cross-plots of the model parameters determined from inversion of TD data representing a homogenous half-space: $\sigma_0 = 10$ mS/m, $m_0 = 100$ mV/V ($\sigma''_{\max} = 0.13$ mS/m), $\tau_\sigma = 0.1$ s, and $C = 0.3$. Two different models have been used for parameterisation of IP: (a–c) the conductivity Cole–Cole model; (d–f) the MIC Cole–Cole model. The red cross marks the true model.

Changing the frequency exponent

To study the influence of the re-parameterisation on models with different resolutions, we have varied the values of C between $C = 0.2$ and $C = 0.6$ in the CCC model, whereas the remaining parameters have been kept constant (i.e., $\sigma_0 =$ 10 mS/m, m, = 100 mV/V, and $\tau_\sigma = 0.1$ *s*). Variation in C in the CCC model gives rise to changes in not just C but also in $\sigma''_{\max}$, $\varphi_{\max}$, $\rho''_{\min}$, τ_φ and τ_ρ in the equivalent re-parameterized models, as these parameters are functions of C and m_0.

As the STDFs of σ_0, ρ_0, τ_φ, τ_σ, τ_ρ, and C do not vary significantly between parameterisations (as seen in Fig. 3) and the CCC and RCC results are equivalent, only the STDFs of m_0, $\varphi_{\max}$, $\sigma''_{\max}$, and $\rho''_{\min}$ are presented in the uncertainty analysis in Table 1.

For TD and FD data, the resolution of m_0, $\varphi''_{\max}$, $\sigma''_{\max}$, and $\rho''_{\min}$ decreases as the value of C is decreased. For $C =$ 0.2, the resolution of $\varphi_{\max}$, $\sigma''_{\max}$, and $\rho''_{\min}$, is close to a 10-fold improvement compared with the resolution of m_0. For $C = 0.4$, the improvement is down to 2-fold in TD. When $C = 0.6$, the uncertainty is approximately the same for all the parameterisations. This shows that especially poorly resolved models benefit from the re-parameterisations, but the impact on well-resolved models is minor.

Changing the noise model

In the following, we show the influence of the noise model on the resolution capabilities of the classic Cole–Cole model compared to that of the re-parameterisations. This is done by assuming different noise levels in the dataset generated from the previous described model. The noise levels on the data-space phase/ chargeability values are: 5% relative noise plus 0.1 (mrad for FD and mV/V for TD) absolute noise, 10% relative noise plus 0.2 mrad/mV/V absolute noise (used in the previous examples), and 15% relative noise plus 0.3 mrad/mV/V absolute noise.

The results of the uncertainty analysis are presented in Table 2 as the STDFs of the marginal posterior probability

Table 1 Uncertainty analysis for different parameterisations and different values of C. Using MCMC inversion, we have analysed five different models where the value of C varied between 0.2 and 0.6, and the remaining parameters have been kept constant: $\sigma_0 = 10$ mS/m, $m_0 = 100$ mV/V, and $\tau_\sigma = 0.1$ *s*. The results are shown for the conductivity Cole–Cole (m_0), the MIC Cole–Cole ($\sigma''_{\max}$), the MIR Cole–Cole ($\rho''_{\min}$), and the MPA Cole–Cole ($\varphi_{\max}$) parameterisation. The uncertainties are given as the STDF of the marginal posterior probability distributions

	Time-domain STDFs				Frequency-domain STDFs			
C	m_0	σ''_{max}	ρ''_{min}	φ_{max}	m_0	σ''_{max}	ρ''_{min}	φ_{max}
0.2	1.7	1.13	1.12	1.11	1.6	1.06	1.07	1.06
0.3	1.4	1.13	1.12	1.11	1.13	1.04	1.04	1.04
0.4	1.2	1.12	1.10	1.10	1.05	1.04	1.04	1.04
0.5	1.11	1.06	1.06	1.05	1.03	1.04	1.04	1.04
0.6	1.07	1.05	1.05	1.05	1.03	1.04	1.04	1.04

Table 2 Uncertainty analysis for different parameterisation and different noise models. The model has the parameters: $\sigma_0 = 10$ mS/m, $m_0 = 100$ *mV/V*, $\tau\sigma = 0.1$ s, and $C = 0.3$. The results are shown from the conductivity Cole–Cole (m_0), the MIC Cole–Cole ($\sigma$$), the MIR Cole–Cole and the MPA Cole–Cole ($\varphi_{\max}$) parameterisations. The uncertainties are given as the STDF of the marginal posterior probability distributions

	Time-domain			Frequency-domain		
	5%	10%	15%	5%	10%	15%
Noise	0.1 mV/V	0.2 mV/V	0.3 mV/V	0.1 mrad	0.2 mrad	0.3 mrad
STDF($\mathbf{m_0}$)	1.2	1.4	1.5	1.05	1.13	1.4
STDF($\sigma''_{\max}$)	1.07	1.13	1.2	1.02	1.04	1.08
STDF($\rho''_{\min}$)	1.05	1.12	1.2	1.02	1.04	1.09
STDF($\phi_{\max}$)	1.06	1.11	1.2	1.02	1.04	1.08

distributions of m_0, $\sigma''_{\max}$, $\rho''_{\min}$, and $\varphi_{\max}$. For all parameterisations, we see that as the noise level is increases, the STDF of the model parameters increases as well. This is also valid for the parameters not shown in the table. The analyses show that the resolution improvements gained from the reparameterisations, which have been documented in the previous figures, are valid for all the different noise levels. For the low noise level, the improvement is between 3-fold and 4-fold for TD and 2-fold for FD. For the high noise level, the improvement is 2.5-fold in TD and 4-fold in FD. As seen with the example in Fig. 3, the resolution improvement gained with the re-parameterisations is less pronounced for the remaining parameters.

A multilayer example

Synthetic TD and FD data generated from a three-layered model have been inverted using the CCC model and the re-parameterisations (MIC, MIR, and MPA). The model was given the CCC model and the re-parameterisations (MIC, MIR and MPA). The model was given the CCC parameters: σ_0 = [50, 50, 50] mS/m, m_0 = [5, 300, 5] mV/V, τ_σ = [0.1, 3, 5] *s*, C = [0.3, 0.3, 0.3] and thickness = [7, 7] m. The data were generated from a vertical sounding with 20 quadrupoles, with electrode spacing |AB| = 7.5–500 m and |MN| = 2.5–65 m.

The inversion results of the TD and FD data show the same features. Furthermore, the MIC, the MIR, and the MPA Cole–Cole models preform equally well. For these reasons, we only present the TD marginal posterior probability distributions of m_0 (CCC) and $\sigma''_{\max}$ (MIC) in Fig. 5.

The inversion results show a 3- to 6-fold improvement in the resolution from m_0 to $\sigma''_{\max}$ in the top and bottom layers where the chargeability is low. It is an improvement from poorly resolved parameters (Fig. 5a and Fig. 5c) to well-resolved parameters (Fig. 5d and Fig. 5f). For the remaining parameters, the differences between the two parameterisations are negligible. In the second layer, the MIC Cole–Cole model produces a slightly lower STDF of $\sigma''_{\max}$ relative to m_0 (Fig. 5b and Fig. 5e), and again, the differences between the parameterisations are negligible for the remaining parameters.

FIELD EXAMPLE

The field data were acquired at the Samsø island (Denmark). The geology at the site is very heterogeneous in the first 10–12 m below the surface, which is characterised by

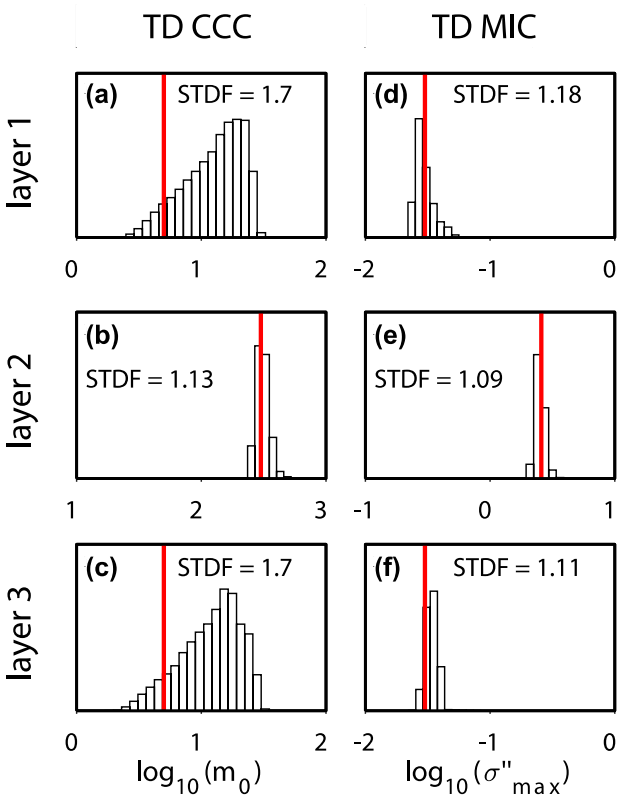

Figure 5 Marginal posterior probability distribution and STDFs for (the conductivity Cole–Cole model) and σ''_{max} (the MIC Cole–Cole model) for the three-layered model: σ_0 = [50, 50, 50] mS/m, m_0 = [5, 300, 5] mV/V, τ_σ = [0.1, 3, 5] *s*, C = [0.3, 0.3, 0.3], and thickness = [7, 7] m. The red line marks the true model values.

late-glacial meltwater deposits and postglacial freshwater sand and peat. Below that, a clay-till layer approximately 20 m thick is present, followed by a regional aquifer in meltwater sand and gravel deposits. Below the regional aquifer, a till/clay layer is present, approximately at 40 m depth. TD IP data were collected along a 2D profile using 49 electrodes with 3 m spacing, for a total length of 144 m. The quadrupole sequence consisted of a mix of gradient and dipole-dipole arrays, for a total of 1161 quadrupoles. Data were acquired using the ABEM Terrameter-LS instrument (www.guidelinegeo.com), with full-waveform signal sampled at 3750 Hz. The full-waveform signal was processed for harmonic de-noising and background drift removal following Olsson *et al.* (2016) and was gated using logarithmically spaced gates from 10^{-3} to 12 s (with 10 points per decade). The de-noised and re-gated TDIP data were imported to the Aarhus Workbench software (www.aarhusgeosoftware.dk) for manual processing of the IP decays. Single gates or entire decays showing poor quality, for instance, due to poor signal-to-noise ratio, were removed. On average, the TD decays have 3.4 decades of usable time range after processing. A 1% standard deviation has been assigned to the resistivity data; 10% relative standard deviation plus 0.05 mV/V absolute noise has been assigned to the IP data. Vertical and horizontal constraints values, expressed as STDFs, were set up to 1.5 and 1.15, respectively.

Figure 6 shows the inversion results for the CCC model. Panels (a–d) represent the uncertainty on the inversion parameters (σ_0, m_0, τ_σ, C) computed following equation (22), using the final inversion model for the Jacobian computation; panels (f–i) show the inversion model, for the σ_0, m_0, τ_σ and C parameters. On top of the (a–d) and (f–i) panels, the DOI is shown as a black line. Panel (e) shows examples of the recorded IP decays with error bars and fitting forward responses (black lines), panel (j) shows the resistivity pseudosection, and panel (k) is the pseudosection of IP data. Panel (l) shows the data misfit of DC data (blue line) and IP data (red line).

Figure 7 shows the results of the MIC inversion, with uncertainty on panels (a–b) and model on panels (f–i) for the inversion parameters σ_0, σ''_{max}, τ_σ, and C. On both Figs 6 and 7 the lithological information available from a nearby borehole is superimposed on the inversion.

The σ_0, τ_σ, and C inversion results are really similar in the CCC and MIC inversion of Figs 6 and 7, in terms of inversion model (panels (f–i)), uncertainty (panels (a–d)), and DOI. Significant differences exist between the m_0 and σ''_{max} results. The uncertainty values decrease with depth much quicker, indicating less resolution at depth. This is reflected also in the DOI estimation that is more than double for the σ''_{max} parameter. Furthermore, a better correlation between geology and σ''_{max} exists, when compared to the m_0 results. The sand layer at 4.0 m depth is better represented in the σ''_{max} section (with values below ~0.05 mS/m), with a superior thickness resolution when compared to the low-m_0 anomaly (with values below ~30 mV/V). Anomalies with high σ''_{max} values (above ~0.15 mS/m) and high m_0 values (above ~70 mV/V) correspond to the till layer (16 m thick) below 8.3 m, but the σ''_{max} anomaly resembles better the geological layer. Finally, the increase in σ''_{max} at depth correlates with the depth of the till/clay layer present below the regional aquifer, at depth of approximately 40 m.

DISCUSSION

The comparison between the classic Cole–Cole model and the re-parameterisations of the Cole–Cole model has been carried

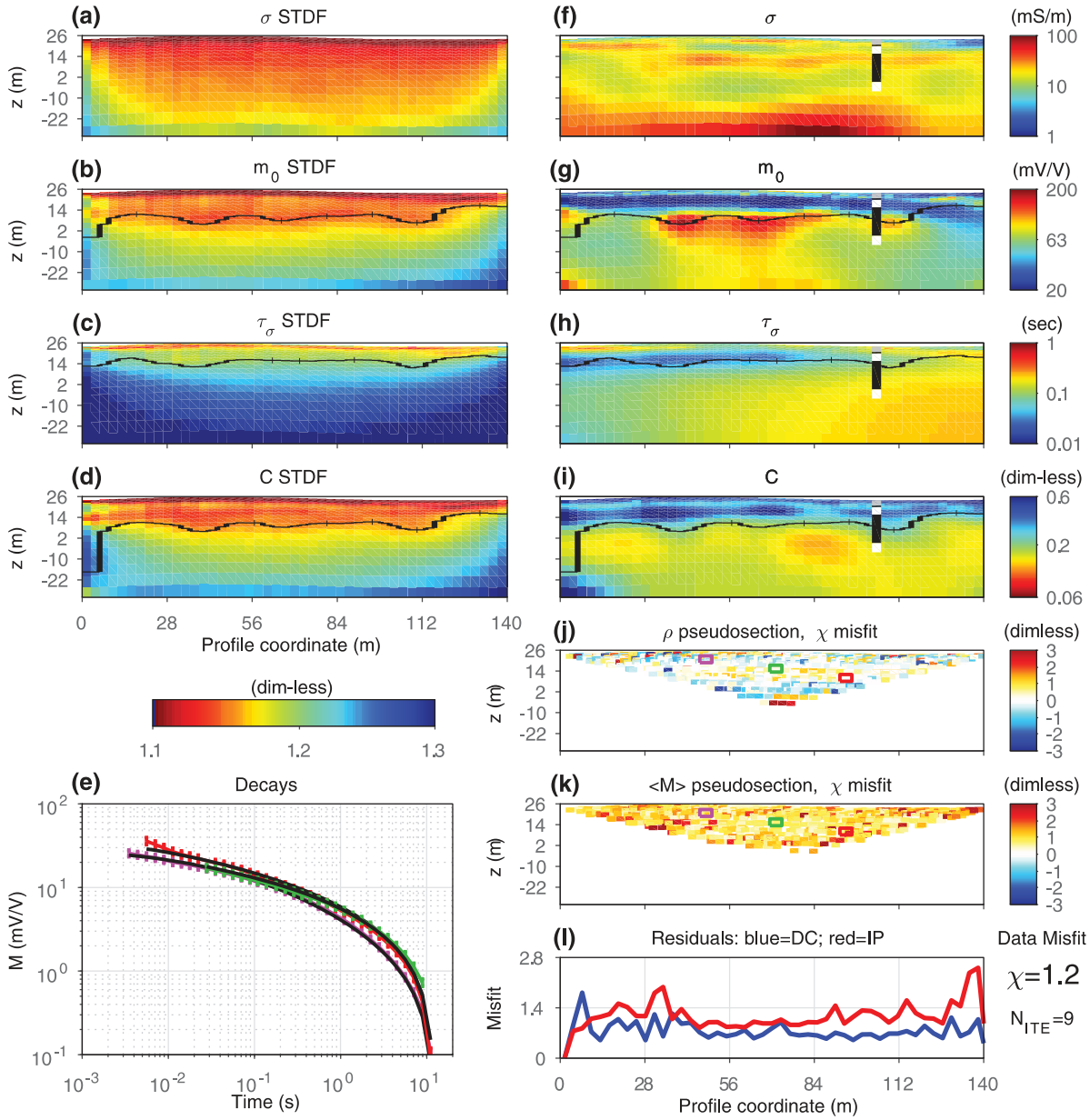

Figure 6 Inversion model, uncertainty analysis, and misfit of field data from Samsø, Denmark, obtained using the conductivity Cole–Cole parameterisation. (a–d) The uncertainty analysis given as the STDF of the four model parameters; (e) three examples of IP decays with error bars (the locations of the data cells are marked in panel (j and k)) and fitting forward response (black lines); (f–i) inversion model with borehole information (white is sand, black is till, and grey is silt); (j) resistivity pseudosection showing the misfit χ; (k) pseudosection of the root mean square χ for the entire IP decay (defined positive); (l) misfit of DC (blue) and IP (red) data of the inversion averaged vertically (and over all the gates for the IP misfit) along the pseudosection. N_{ITE} is the number of iterations. The black lines in panels (a–d) and (f–i) are the DOI.

out on both TD and FD IP data, but it is beyond the scope of this study to present a complete comparison of the TD and FD IP methods. In fact, the settings of the TD and FD data generation are selected focusing on getting equivalent acquisition ranges, but a TD/FD comparison study should also take other factors into account, e.g., the acquisition range actually measurable in the lab/field. Despite the same number of decades (approximately 3.5 decades) being used for both TD and FD synthetic data generation, we see that the two methods are not focused at the exact same

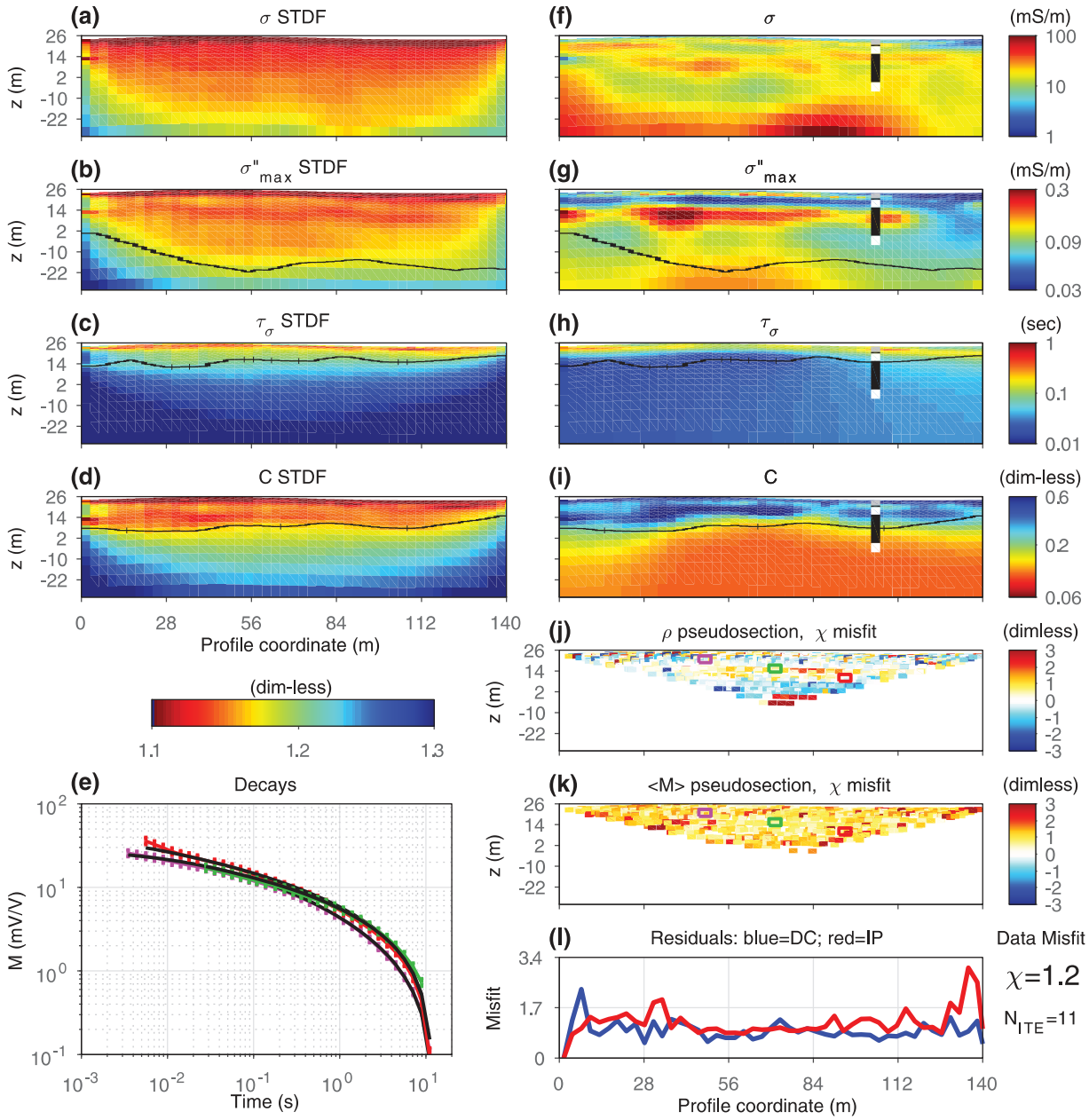

Figure 7 Inversion model, uncertainty analysis, and misfit of field data from Samsø, Denmark, obtained using the MIC Cole–Cole model for parameterisation of IP. (a–d) The uncertainty analysis given as the STDF of the four model parameters; (e) three examples of IP decays with error bars (the locations of the data cells are marked in panel (j and k)) and fitting forward response (black lines); (f–i) inversion model with borehole information (white is sand, black is till, and grey is silt); (j) resistivity pseudosection showing the misfit χ; (k) pseudosection of the root mean square χ for the entire IP decay (defined positive); (l) misfit of DC (blue) and IP (red) data of the inversion averaged vertically (and over all the gates for the IP misfit) along the pseudosection. N_{ITE} is the number of iterations. The black lines in panels (a–d) and (f–i) are the DOI.

spectral range. Indeed, for $\tau = 0.1\ s$ (the results presented in this study), we see that the synthetic FD data often resolve the model parameters better than the TD data. However, for $\tau = 0.1\ s$, the situation is the opposite and the TD data give the best resolution. With these remarks, the TD and the FD methods show approximately the same improvements with the application of the re-parameterised Cole–Cole models.

The MPA, MIC, and MIR models show similar results in terms of uncertainty analysis. However, the MPA modelling has an advantage when compared to the MIC and the MIR parameterisations. Indeed, the φ_{max} parameter directly controls the magnitude of the IP response, whereas in the MIC and MIR model, the response magnitude depends on the σ''_{max}/σ_0 and ρ''_{min}/ρ_0 ratios, respectively.

On the other hand, many petrophysical relations involving IP properties are expressed in terms of real/imaginary conductivity, for instance, the linear relation between the real and imaginary surface conductivity described by Weller, Slater, and Nordsiek (2013) or the relation between hydraulic permeability and real and imaginary conductivity found by Weller *et al.* (2015). In this respect, the MIC model is more suited for applying petrophysical relations directly from the inversion results. A final consideration can be made about the comparison of field and laboratory IP results. Typically, laboratory IP measurements are carried out in FD, and the results are shown in terms of amplitude/phase and/or real/imaginary conductivity. In this respect, inversions of field data in terms of MPA or MIC models are much easier to compare with laboratory results in comparison to classic Cole–Cole or MIR inversions.

CONCLUSION

We have derived and tested three re-parameterisation of the Cole–Cole model for the inversion of TDIP and FDIP data, namely the MPA Cole–Cole model $\{\rho_0, \varphi_{max}, \tau_\varphi, C\}$, the MIC Cole–Cole model $\{\sigma_0, \sigma''_{max}, \tau_\sigma, C\}$, and the MIR Cole–Cole model $\{\rho_0, \rho''_{min}, \tau_\rho, C\}$.

The uncertainty analyses of synthetic homogenous half-space models and multilayered model, which were computed using the MCMC method, show that the MPA, MIC, and MIR Cole–Cole parameters, compared with the classic Cole–Cole parameters, are less correlated in the inversion of both FD and TD IP data. Consequently, we see that the re-parameterisations increase the resolution of the model parameters, specifically of the φ_{max}, σ''_{max}, and ρ''_{min} parameters in comparison with the classic m_0 parameter. The resolution improvement obtained by the re-parameterisations is especially significant for models with low C values or low signal-to-noise ratio (i.e., models that are poorly resolved using the classic Cole–Cole model), where 3-fold improvements or better are observed. The resolution improvements are less pronounced or absent for models that are well resolved with the classic Cole–Cole model.

A 2D field example where we compare the classic Cole–Cole and the MIC models shows that gradient-based inversion methods benefit from the re-parameterisations as well. A significantly deeper (more than double) DOI was found for σ''_{max} in comparison with the classic m_0, together with a better correlation with geology.

Consequently, it is recommended to invert for one of the re-parameterisations of the Cole–Cole model in any Cole–Cole inversion of IP data and then, if needed, transform the parameters back to the classic parameterisation. In particular, we believe that the MPA and the MIC parameterisations will be particularly effective for the spectral inversion of field IP data and will contribute to narrow the gap among IP theory, laboratory findings, and field applications.

ACKNOWLEDGEMENT

This work was cofounded by the project GEOCON (Advancing GEOlogical, geophysical and CONtaminant monitoring technologies for contaminated site investigation; www.geocon.env.dtu.dk).

REFERENCES

Auken E., Christiansen A.V., Jacobsen B.H., Foged N. and Sørensen K.I. 2005. Piecewise 1D laterally constrained inversion of resistivity data. *Geophysical Prospecting* **53**, 497–506.

Bérubé C.L., Chouteau M., Shamsipour P., Enkin R.J. and Olivo G.R. 2017. Bayesian inference of spectral induced polarization parameters for laboratory complex resistivity measurements of rocks and soils. *Computers & Geosciences* **105**, 51–64.

Binley A., Slater L.D., Fukes M. and Cassiani G. 2005. Relationship between spectral induced polarization and hydraulic properties of saturated and unsaturated sandstone. *Water Resources Research* **41**, 1–13.

Börner F.D., Schopper J.R. and Weller A. 1996. Evaluation of transport and storage properties in the soil and groundwater zone from induced polarization measurements. *Geophysical Prospecting* **44**, 583–601.

Chen J., Kemna A. and Hubbard S.S. 2008. A comparison between Gauss-Newton and Markov-chain Monte Carlo-based methods for inverting spectral induced-polarization data for Cole–Cole parameters. *Geophysics* **73**, F247-F259.

Cole K.S. and Cole R.H. 1941. Dispersion and absorption in dielectrics. *Journal of Chemical Physics* **9**, 341–351.

Fiandaca G., Auken E., Gazoty A. and Christiansen A.V. 2012. Time-domain induced polarization: full-decay forward modeling and 1D laterally constrained inversion of Cole–Cole parameters. *Geophysics* **77**, E213–E225.

Fiandaca G., Christiansen A. and Auken E. 2015. Depth of investigation for multi-parameters inversions. Near Surface Geoscience 2015–21st European meeting of environmental and engineering geophysics.

Fiandaca G., Ramm J., Binley A., Gazoty A., Christiansen A.V. and Auken E. 2013. Resolving spectral information from time

domain induced polarization data through 2-D inversion. *Geophysical Journal International* **192**, 631–646.
Gazoty A., Fiandaca G., Pedersen J., Auken E. and Christiansen A.V. 2012. Mapping of landfills using time-domain spectral induced polarization data: the Eskelund case study. *Near Surface Geophysics* **10**, 575–586.
Hastings W.K. 1970. Monte Carlo sampling methods using Markov chains and their applications. *Biometrika* **57**, 97–109.
Hönig M. and Tezkan B. 2007. 1D and 2D Cole–Cole inversion of time-domain induced-polarization data. *Geophysical Prospecting* **55**, 117–133.
Johansson S., Fiandaca G. and Dahlin T. 2015. Influence of non-aqueous phase liquid configuration on induced polarization parameters: conceptual models applied to a time-domain field case study. *Journal of Applied Geophysics* **123**, 295–309.
Johansson S., Sparrenbom C., Fiandaca G., Lindskog A., Olsson P.-I., Dahlin T. and Rosqvist H. 2016. Investigations of a Cretaceous lime-stone with spectral induced polarization and scanning electron microscopy. *Geophysical Journal International*, ggw432.
Kemna A., Binley A. and Slater L. 2004. Crosshole IP imaging for engineering and environmental applications. *Geophysics* **69**, 97–107.
Leroux V., Dahlin T. and Svensson M. 2007. Dense resistivity and induced polarization profiling for a landfill restoration project at Härlöv, Southern Sweden. *Waste Management & Research* **25**, 49–60.
Loke M.H., Chambers J.E. and Ogilvy R.D. 2006. Inversion of 2D spectral induced polarization imaging data. *Geophysical Prospecting* **54**, 287–301.
Madsen L.M., Fiandaca G., Auken E. and Christiansen A.V. 2017. Time-domain induced polarization—An analysis of Cole–Cole parameter resolution and correlation using Markov chain Monte Carlo inversion. *Geophysical Journal International*.
Malinverno A. 2002. Parsimonious Bayesian Markov chain Monte Carlo inversion in a nonlinear geophysical problem. *Geophysical Journal International* **151**, 675–688.
Maurya, P. K., Fiandaca, G., Auken, E. and Christiansen, A. V. 2016. Lithological characterization of a comtaminated site using direct current resistivity and time domain induced polarization. IP2016/4th International Workshop on Induced Polarization, 6.-8. Aarhus, Denmark, June 2016.
Metropolis N., Rosenbluth A.W., Rosenbluth M.N., Teller A.H. and Teller E. 1953. Equation of state calculations by fast computing machines. *The Journal of Chemical Physics* **21**, 1087–1092.
Mosegaard K. and Tarantola A. 2002. Probabilistic approach to inverse problems. In: *International Handbook of Earthquake and Engineering Seismology* (eds W. Lee, P. Jennings, C. Kisslingers, and H. Kanamori). Academic Press.
Nordsiek S., Diamantopoulos E., Hördt A. and Durner W. 2016. Relationships between soil hydraulic parameters and induced polarization spectra. *Near Surface Geophysics* **14**, 23–37.
Olsson P.-I., Fiandaca G., Larsen J.J., Dahlin T. and Auken E. 2016. Doubling the spectrum of time-domain induced polarization by harmonic de-noising, drift correction, spike removal, tapered gating and data uncertainty estimation. *Geophysical Journal International* **207**, 774–784.
Olsson P.I., Dahlin T., Fiandaca G. and Auken E. 2015. Measuring time-domain spectral induced polarization in the on-time:decreasing acquisition time and increasing signal-to-noise ratio. *Journal of Applied Geophysics* **2015**, 6.
Pelton W.H., Ward S.H., Hallof P.G., Sill W.R. and Nelson P.H. 1978. Mineral discrimination and removal of inductive coupling with multi-frequency IP. *Geophysics* **43**, 588–609.
Seigel H.O. 1959. Mathematical formulation and type curves for induced polarization. *Geophysics* **24**, 547–565.
Slater L.D. and Lesmes D. 2002. IP interpretation in environmental investigations. *Geophysics* **67**, 77–88.
Tarantola A. and Valette B. 1982. Generalized nonlinear inverse problems solved using a least squares criterion. *Reviews of Geophysics and Space Physics* **20**, 219–232.
Tarasov A. and Titov K. 2013. On the use of the Cole–Cole equations in spectral induced polarization. *Geophysical Journal International* **195**, 352–356.
Vanhala H. 1997. Mapping oil-contaminated sand and till with the spectral induced polarization (IP) method. *Geophysical Prospecting* **45**, 303–326.
Weller A., Slater L., Binley A., Nordsiek S. and Xu S. 2015. Permeability prediction based on induced polarization: insights from measurements on sandstone and unconsolidated samples spanning a wide permeability range. *Geophysics* **80**, D161–D173.
Weller A., Slater, L. & Nordsiek, S. 2013. On the relationship between induced polarization and surface conductivity: Implications for petrophysical interpretation of electrical measurements. *Geophysics* **78**, D315-D325.
Yoshioka K. and Zhdanov M.S. 2005. Three-dimensional nonlinear regularized inversion of the induced polarization data based on the Cole–Cole model. *Physics of the Earth and Planetary Interiors* **150**, 29–43.
Yuval and Oldenburg D.W. 1997. Computation of Cole–Cole parameters from IP data. *Geophysics* **62**, 436–448.

APPENDIX A

From MPA Cole–Cole to classic Cole–Cole

Given the MPA Cole–Cole model parameters $\{\rho_0, \varphi_{\max}, \tau_\varphi, C\}$, the corresponding parameters of the resistivity (or conductivity) Cole–Cole model $\{\rho_0, m_0, \tau_\rho, C\}$ can be computed through the following iterative approach.

As a start, we define the variables and as follows:

$$a(\omega) = Re\left(\frac{1}{1+(i\omega\tau_\rho)^C}\right) \tag{A.1}$$

$$b(\omega) = Im\left(\frac{1}{1+(i\omega\tau_\rho)^C}\right), \tag{A.2}$$

Table B.1 IP gating

Gate	1	2	3	4	5	6	7	8	9	10	11	12	13
Gate width (ms)	1.06	1.33	2.13	2.93	4	5.33	7.46	10.4	14.4	20	20	40	60
Gate	14	15	16	17	18	19	20	21	22	23	24	25	26
Gate width (ms)	80	100	140	200	280	380	540	760	1040	1460	2020	2800	2000

Table B.2 Acquisition frequencies

Frequencies (Hz)												
0.08	0.16	0.32	0.64	1.28	2.56	5.12	10.2	20.4	40.9	81.9	163	327

where *Re* and *Im* indicate the computation of the real and imaginary part of a complex number, respectively. Thus, equation (1) can be written as follows:

$$\tilde{\rho}(\omega) = \rho_0[1 - m_0(1 - (a(\omega) + ib(\omega)))]. \tag{A.3}$$

We now iterate to minimise the following:

$$\Delta m_0 = \frac{|m_0(n) - m_0(n-1)|}{m_0(n)}, \tag{A.4}$$

where $m_0(0) = 0$. For the nth iteration, $\tau_\rho(n)$ and $m_0(n)$ are computed as follows:

$$\tau_\rho(n) = \tau_\varphi \cdot (1 - m_0(n-1))^{-1/2C} \tag{A.5}$$

$$a(n) = Re\left(\frac{1}{1 + \left(i\frac{\tau_\rho(n)}{\tau_\varphi}\right)^C}\right) \tag{A.6}$$

$$b(n) = Im\left(\frac{1}{1 + \left(i\frac{\tau_\rho(n)}{\tau_\varphi}\right)^C}\right) \tag{A.7}$$

$$m_0(n) = \frac{tan(-\varphi_{max})}{(1 - a(n)) \cdot tan(-\varphi_{max}) + b(n)}. \tag{A.8}$$

Once the classic Cole–Cole parameters $\{\rho_0, m_0, \tau_\rho, C\}$ are defined in terms of the MPA parameters $\{\rho_0, \varphi_{\max}, \tau_\varphi, C\}$, the Cole–Cole complex resistivity (or conductivity) can be computed through equation (1) (or equation (3)) at any frequency.

From MIC Cole–Cole to classic Cole–Cole

Given the MIC Cole–Cole model parameters $\{\sigma_0, \sigma''_{\max}, \tau_\sigma, C\}$, the corresponding parameters of the resistivity (or conductivity) Cole–Cole model $\{\rho_0, m_0, \tau_\rho, C\}$ can be computed directly. As a start, we define the variable d as:

$$d = Im\left(\frac{1}{1 + (1i)^C}\right) \tag{A.9}$$

The chargeability of the Cole–Cole model, m_0, is then given as follows:

$$m_0 = \frac{\sigma''_{\max}}{(\sigma''_{\max} - \sigma_0 \cdot d)}. \tag{A.10}$$

The relaxation time in the resistivity form, τ_ρ, can now be computed from equation (5)

From MIR Cole–Cole to classic Cole–Cole

Given the MIR Cole–Cole model parameters $\{\rho_0, \rho''_{\min}, \tau_\rho, C\}$, the corresponding parameters of the resistivity (or conductivity) Cole–Cole model $\{\rho_0, m_0, \tau_\rho, C\}$ can be computed directly as follows:

$$m_0 = -\frac{\rho''_{\min}}{(\rho_0 \cdot d)}, \tag{A.11}$$

where d is as defined in equation (A.9).

APPENDIX B

Gating of TDIP signal

The gating of the transient IP signal, which is recorded from 2.6 ms to 12,000 ms, is listed in Table B.1

Acquisition frequencies

The frequencies used for the computation of synthetic FD IP forward responses are listed in Table B.2